

pubs.acs.org/JPCB Article

Structure—Dynamics Interrelation Governing Charge Transport in Cosolvated Acetonitrile/LiTFSI Solutions

Murillo L. Martins,* Xiaobo Lin, Catalin Gainaru, Jong K. Keum, Peter T. Cummings, Alexei P. Sokolov, Robert L. Sacci, and Eugene Mamontov*



Cite This: J. Phys. Chem. B 2023, 127, 308–320



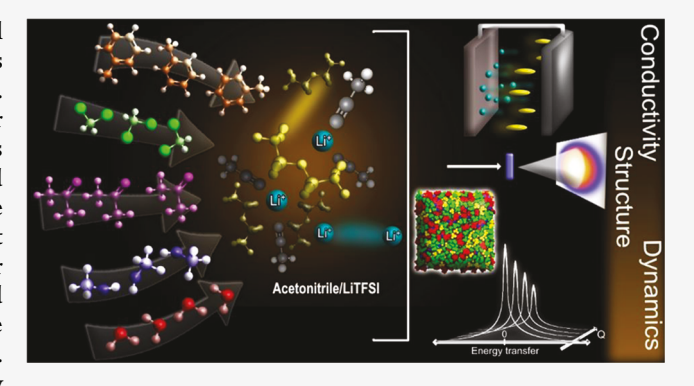
ACCESS I

III Metrics & More



Supporting Information

ABSTRACT: Concentrated ionic solutions present a potential improvement for liquid electrolytes. However, their conductivity is limited by high viscosities, which can be attenuated via cosolvation. This study employs a series of experiments and molecular dynamics simulations to investigate how different cosolvents influence the local structure and charge transport in concentrated lithium bis(trifluoromethane-sulfonyl)imide (LiTFSI)/acetonitrile solutions. Regardless of whether the cosolvent's dielectric constant is low (for toluene and dichloromethane), moderate (acetone), or high (methanol and water), they preserve the structural and dynamical features of the cosolvent-free precursor. However, the dissimilar effects of each case must be individually interpreted. Toluene and dichloromethane reduce the conductivity by



narrowing the distribution of Li⁺-TFSI⁻ interactions and increasing the activation energies for ionic motions. Methanol and water broaden the distributions of Li⁺-TFSI⁻ interactions, replace acetonitrile in the Li⁺ solvation, and favor short-range Li⁺-Li⁺ interactions. Still, these cosolvents strongly interact with TFSI⁻, leading to conductivities lower than that predicted by the Nernst-Einstein relation. Finally, acetone preserves the ion-ion interactions from the cosolvent-free solution but forms large solvation complexes by joining acetonitrile in the Li⁺ solvation. We demonstrate that cosolvation affects conductivity beyond simply changing viscosity and provide fairly unexplored molecular-scale perspectives regarding structure/transport phenomena relation in concentrated ionic solutions.

■ INTRODUCTION

Concentrated solutions of Li salts are among the most promising classes of next-generation liquid electrolytes. Typically, solutions with salt/solvent weight or volume ratios >1^{1,2} have been intensively explored since such a concentrated regime leads to unique solvation structures and physicochemical properties.³ At this condition, very few solvent molecules do not participate in the ionic coordination, and highly crowded solvation sheaths, also populated by the anions, may be formed around the cations.⁴ Typically, these arrangements are charge-balanced by uncoordinated anions and/or smaller and less predominant solvation complexes and, thanks to these stable ion—ion and ion—solvent interplays, highly concentrated solutions are often regarded as solvated ionic liquids.^{4,5}

As electrolytes, concentrated solutions of Li salts may provide high thermal, chemical, and cycling stabilities, ^{2,6} low volatility, and allow for large electrochemical voltage windows to be achieved. ^{1,7} However, the high salt concentration itself brings drawbacks, such as high costs, salt precipitation at low temperatures, and high viscosity, which may kinetically inhibit intercalation in electrode materials and reduce overall device performance. ^{8–10} To bypass these obstacles, the addition of

soluble cosolvents to the concentrated systems is a sound alternative as one can, for example, lower the solution's viscosity while preserving (or even enhancing) certain physicochemical properties of the original solution. Low-polar cosolvents with low dielectric constants have been mostly used since they scarcely engage in ionic coordination and are expected to be electrochemically inert. This approach has been used with the addition of cosolvents based on hydrofluoroether to solutions of lithium bis-(trifluoromethane-sulfonyl)imide (LiTFSI) in glymes and of lithium tetrafluoroborate (LiBF4) in propylene carbonates. In both cases, the cosolvation allowed for the original solvation structures and anodic stabilities to be maintained. Similarly, benefits related to the performance and stabilization of batteries have been achieved with concentrated solutions of

Received: October 18, 2022 Revised: December 5, 2022 Published: December 28, 2022





sodium (fluorosulfonyl)imide (NaFSI) in 1,2-dimethoxyethane (DME) and LiFSI in dimethyl carbonate and tetramethylene sulfone cosolvated with fluorinated ethers. 16,17 Chloroform has also been used as a cosolvent in an acetonitrile/LiTFSI solution and enabled higher specific capacitance and reduced resistivity in carbon electrodes. 13 As a drawback, the addition of cosolvents with low dielectric constants may promote the formation of large ionic aggregates, which has been pointed out as the main reason for a reduction in room-temperature conductivity. 9,13 As discussed in this study, however, additional effects may also contribute to this outcome. The addition of polar cosolvents with high dielectric constants may lead to ligand exchange in the first solvation shell, which increases the number of uncoordinated molecules in the system and decreases the electrochemical window. 18 Still, cosolvents with physicochemical properties somewhat comparable to those of the main solvent can be used. In this case, although ligand exchange may still occur, the formation of ionic aggregates is not directly promoted, but ionic correlations, characteristic of concentrated solutions, still occur via long-range interactions. 19 Hence, at least three cosolvation mechanisms may prevail depending on the cosolvent's properties.

Besides their practical applications, concentrated Li solutions are also interesting for the fundamental understanding of charge transport in highly concentrated electrolytes because of their unusual mechanisms of ion diffusion. In many cases, the behavior of these systems cannot be solely explained by a vehicular mechanism (the charge being transported by molecular fragments as vehicles) since decoupling between charge mobility and diffusivity and/or conductivity and viscosity may occur. For rationalizing this decoupling, microscopic diffusion mechanisms have been suggested based on ligand exchange, formation of bulk-like diffusive channels, establishment of percolating networks, Li+ hopping, and others.31-35 For these mechanisms, the role played by the coordination structure, that is the close-contact ion-ion and ion-solvent correlations, as well as correlations with longer ranges, have been debated. Hence, in the present work, we extend these discussions to cosolvated systems and reveal that the interplay between both close-contact and long-range interactions must be considered to explain the charge transport in these solutions.

Specifically, we report a comprehensive study on the ionion and ion-solvent interactions within a concentrated LiTFSI/acetonitrile solution cosolvated with compounds with low (toluene and dichloromethane), moderate (acetone), and high (methanol and water) dielectric constants, as listed in Table 1. We combine several experimental techniques including dielectric spectroscopy, rheology, X-ray scattering, infrared (IR) spectroscopy, and quasi-elastic neutron scattering (QENS), with molecular dynamics (MD) simulations. Regardless of the cosolvents' dielectric constants, it appears that the resulting electrolytes preserve characteristics of concentrated systems, including the degree of ion-ion correlations found in the cosolvent-free solution. However, while equally abundant, these correlations have different natures depending on the cosolvent and so do also the ionsolvent interactions. Toluene and dichloromethane diminish the room-temperature conductivity by promoting a less dispersed character to the Li+-TFSI- close-contact interactions and increasing the activation energies for ionic motions. Meanwhile, methanol, and especially water, promote a disordered character to the Li⁺-TFSI⁻ interactions and a

Table 1. Solvents Used to Prepare the Cosolvated LiTFSI/Acetonitrile Solutions with the Respective Specifications^a

cosolvent	dielectric constant (ε) at 25 °C	dipole moment (liquid state) (D)	molar weight (g/mol)	density (kg/m³)	viscosity (mPa·s) at 25 °C
acetonitrile	36.0^{21}	4.50 ²²	41.05	786	0.34
toluene	2.40^{23}	0.36^{24}	92.14	863	0.56
dichloromethane	8.85^{25}	1.83^{26}	84.93	1330	0.41
acetone	21.2^{21}	3.56^{27}	58.08	784	0.31
methanol	33.1^{21}	2.60^{28}	32.04	786	0.54
water	78.4^{29}	2.90^{30}	18.01	997	0.89

^aData from ref 20 unless indicated otherwise.

prominent solvent exchange in the Li⁺ solvation. However, the strong interactions between these cosolvents and TFSI⁻ prevent these systems from exhibiting conductivities as high as expected. Finally, acetone, whose dielectric constant is moderate compared with that of acetonitrile, promotes intermediary mechanisms as the resulting ion—ion and ion—solvent interactions are comparable to those in the cosolvent-free solution even if acetone molecules are incorporated into the cations' solvation.

MATERIALS AND METHODS

Preparation of Materials and Samples. Acetonitrile, the cosolvents listed in Table 1, and LiTFSI were purchased from Sigma-Aldrich. All solvents were stored over freshly activated 4 Å molecular sieves for at least 24 h before use, and LiTFSI was dried at 100 °C under vacuum for at least 3 days before preparing the solutions. The solutions were prepared in an argon glovebox by dissolving LiTFSI in acetonitrile in a concentration of 8.1 mol/kg (mols of salt per kilogram of solvent), that is an acetonitrile/LiTFSI = 3:1 molar ratio, and allowed to stabilize for 30 min. The cosolvents were then added to reach a final concentration of 5.5 mol/kg, and the resulting solutions were allowed to stabilize for 3 h before the experiments. The final cosolvent/LiTFSI/acetonitrile ratios are displayed in Table 2.

Table 2. Final Cosolvent/LiTFSI/Acetonitrile Molar Ratios of the Solutions

	cosolvent	LiTFSI	acetonitrile
toluene	0.63	1	3
dichloromethane	0.68	1	3
acetone	1	1	3
methanol	1.8	1	3
water	3.2	1	3

Conductivity Experiments. Conductivity measurements were performed on an Alpha-A analyzer from Novocontrol in the frequency range of 10^{-1} to 10^6 Hz between 190 and 340 K. The samples were placed in a cell containing two parallel electrodes with a diameter of 10.2 mm. Voltages with the maximal amplitudes of 0.1 V have been applied across an electrode distance of 0.4 mm. A Quattro temperature controller (Novocontrol) was used for stabilizing the sample temperature to an accuracy within ± 0.2 K.

Wide-Angle X-ray Scattering (WAXS). Wide-angle X-ray scattering (WAXS) measurements were carried out on a Xenocs Xeuss 3.0 instrument equipped with a D2+ MetalJet X-

ray source (Ga K_{α} , $\lambda = 1.3414$ Å). The samples were aligned perpendicular to the direction of the X-ray beam (transmission mode) and the scattered beam was recorded on a Dectris Eiger 2R 4M hybrid photon counting detector with a pixel dimension of 75 \times 75 μ m². The sample-to-detector distance was 55 mm. This configuration allowed for the momentum transfer range $Q = 0.17-5.1 \text{ Å}^{-1}$ to be covered. The solutions were loaded in quartz capillary cells with a 2 mm inner diameter and sealed with epoxy resin, and the measurements were performed under ambient conditions. The collected twodimensional (2D) WAXS images were circularly averaged and expressed as intensity versus Q, where $Q = (4\pi \sin \theta)/\lambda$ after subtraction of background scattering, where the X-ray exposure time was 600 s. The data were normalized to the incoming beam intensity for absolute scale calibration, and the contributions from the quartz cells were subtracted.

Infrared (IR) Spectroscopy. IR measurements were performed at room temperature with an Agilent Cary 680 spectrometer equipped with a diamond attenuated total reflection accessory (GoldenGate, Specac) at a resolution of 2 cm⁻¹.

Quasi-Elastic Neutron Scattering (QENS) Measurement and Analysis. QENS experiments were conducted at the backscattering spectrometer BASIS³⁶ at the Spallation Neutron Source, Oak Ridge National Laboratory. For these experiments, the solutions were prepared either with protiated (p-)acetonitrile in combination with deuterated (d-) cosolvents or with d-acetonitrile in combination with p-cosolvents. By doing so, the discrepancy between the neutron incoherent cross sections of ¹H and ²D was exploited to evaluate the dynamical behavior of the protiated compounds, while the contributions from the deuterated ones to the collected data are nearly negligible.³⁷ The solutions were loaded into flat aluminum plates with a thickness of 0.25 mm and sealed with indium wires in an Ar-filled glovebox. QENS spectra were collected at 20, 260, 280, and 300 K with an instrumental resolution of 3.7 μ eV. A vanadium standard sample was used as the instrumental resolution. The collected data were reduced with the software Mantid³⁸ following routine procedures (normalization to a flat-plate vanadium standard, subtraction of the instrumental background using the data collected from an empty sample holder, and application of a mask file to exclude noisy detector) and the analyses were performed using the fitting packages qClimax^{39,40} and DAVE.⁴

Molecular Dynamics (MD) Simulations. Details of the MD simulations are presented in Section S1. The simulations were initialized with mBuild^{42,43} (using PACKMOL⁴⁴) and parameterized with foyer and GAFF-foyer software packages.^{45,46} Both software packages fall under the Molecular Simulation and Design Framework (MoSDeF)^{47,48} suite of tools. The whole simulation workflow was managed through the signac Framework.^{49–51} In the course of the simulations, partial charges were assigned with RESP through the use of the R.E.D. Server and Gaussian 09,⁵² following concepts presented in refs 53–55. Once initialized and parametrized, the simulations were performed with GROMACS 2020⁵⁶ and the analyses of self-diffusivities and radial distribution functions (RDFs) were made with MDTraj.^{57,58}

■ RESULTS

Conductivity and Viscosity Measurements. Temperature-dependent conductivity data are presented in Figure 1a for the acetonitrile/LiTFSI solutions with the different

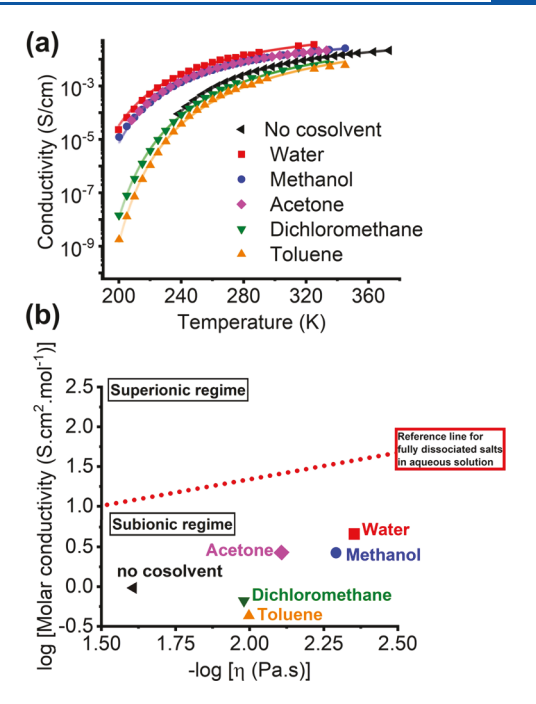


Figure 1. (a) Temperature-dependent conductivity measurements of acetonitrile/LiTFSI solutions (3:1 molar ratio) with different cosolvents. (b) Walden plot of acetonitrile/LiTFSI solutions with different cosolvents. The red dashed line refers to the ideal case corresponding to a dilute aqueous solution.

cosolvents. The lines in the figure represent fits with the Vogel-Fulcher-Tammann (VFT) expression, which is usually employed for ions diffusing through viscous media⁵⁹ and describes well the data for all solutions in the entire investigated dynamic range. In Figure 1b, the molar conductivities at room temperature ($\Lambda = \sigma/c$, where c is the molar concentration) are displayed as a function of the reciprocal viscosities (η^{-1}) (fluidity) of each system. Fully dissociated salts follow Walden's Law ($\Delta \eta = \text{constant}$) as indicated by the red dash line in Figure 1b that presents the ideal line normalized by molar conductivity of dilute aqueous LiCl solution. 60,61 All of the Walden products calculated in the present work are below this ideal line, in the so-called subionic regime in which either not all of the available ions participate in the conductivity process or their diffusion is slower than expected at the given viscosity. In comparison with the cosolvent-free solution, the fluidities increase with the addition of cosolvents with low dielectric constants (toluene and dichloromethane), but the corresponding conductivities decrease. Meanwhile, the addition of acetone, methanol, and water increases both the fluidities and the conductivities compared with the original solution. Interestingly, however, changing the cosolvent from acetone to methanol leads to an increase in fluidity but with no benefits in conductivity. For these cases, as shown in Figure 1a, the conductivities are fairly superposed in the entire temperature range assessed by our experiments. Finally, the addition of water leads to a solution with the Walden product being somewhat closer to the reference line of a dilute system among all of the solutions.

Intermediate-Range Atomic Ordering: Wide-Angle X-ray Scattering (WAXS) and Radial Distribution Functions (RDF). While referring to the structure of the solutions in this work, we consider both a short-range arrangement, defined by the coordination of the ions by the solvents as well

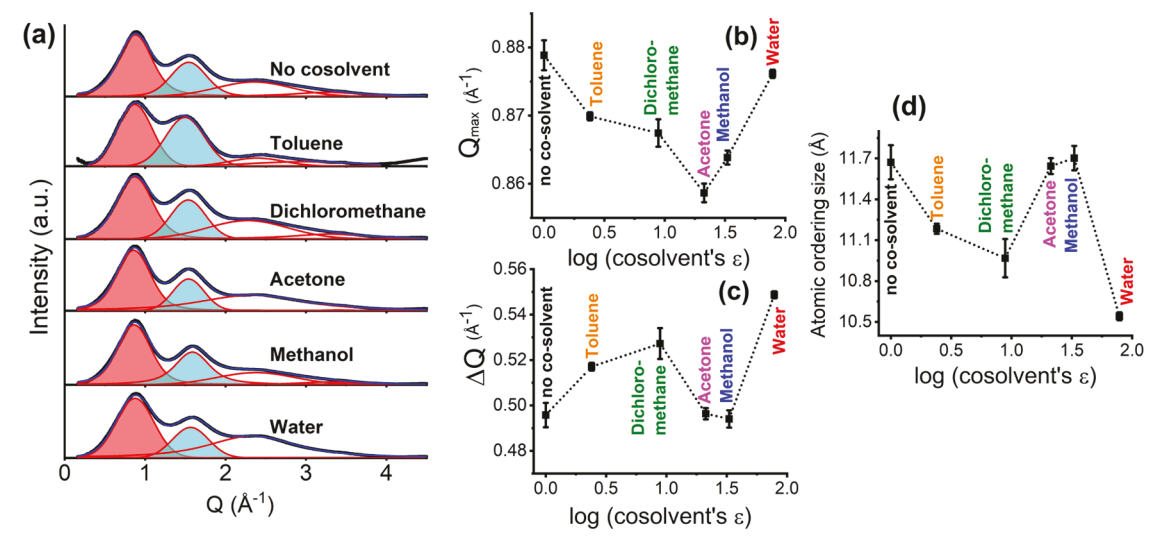


Figure 2. Results obtained with wide-angle X-ray scattering (WAXS) for acetonitrile/LiTFSI solutions (3:1 molar ratio) with different cosolvents. (a) Fit of the main Bragg reflections with Voigt functions. The red-shaded peak is assigned to an intermediate-range atomic ordering within the solutions, the blue-shaded peaks arise from correlations between the solvent molecules and the respective nearest neighbors, and the nonshaded peaks are likely part of the TFSI⁻ molecule's structure factor. (b) Position of the reflections from the intermediate-range atomic ordering (Q_{max}) as extracted by fitting the peaks with a Voigt function. (c) Widths of the reflections from the intermediate-range atomic ordering (ΔQ). (d) Atomic ordering sizes calculated with Scherrer's equation; see text for details.

as ion-ion interactions, and an intermediate-range atomic organization, whose dimensions are beyond the ions' first solvation sheath. We investigated the room-temperature intermediate-range ordering within the electrolytes using WAXS and the corresponding intensity patterns were fitted with a sum of Voigt functions (see Figure 2a). All of the solutions present three categories of Bragg reflections, as also observed in the respective structure factors obtained via MD (see Figure S4). Shaded in blue, the peaks centered around Q = 1.5 Å^{-1} arise from nearest neighbors correlations and, as shown in Figure S4, can also be found in the neat solvents. These reflections are sensitive to the properties of the solvents (such as the size and polarity of their molecular constituents) and are not of particular interest in our work. At Q-values greater than 2.5 Å⁻¹, the nonshaded reflections are within the order of intramolecular correlations (≤2.5Å in real space according to $d = \frac{2\pi}{Q}$) and are likely related to the partial structure factor of TFSI⁻, as they are not detected in the neat solvents (see Figure S4). For the solutions with no cosolvents and with toluene and dichloromethane, additional Pseudo-Voigt components were needed to fit these reflections. Therefore, the discussions regarding the width and position of this peak in the cosolvent-free system and the solutions with toluene and dichloromethane are limited. Still, as described in the Supporting Information (SI) (Figure S4), a meaningful difference can be observed in the broadening of this reflection between the solutions with acetone and methanol, thus suggesting that the flexible molecules of TFSI- can undergo intramolecular changes depending on the cosolvents. Finally, the red-shaded reflections at $Q < 1 \text{ Å}^{-1}$ are assigned to the above-mentioned intermediate-range atomic ordering whose dimensions in real space surpass 7 Å. Qian et al. 63 ascribed this atomic arrangement to a charge-ordering process where the anions and cations are strongly coordinated. Complementary, Lundin et al.⁶² highlighted the contribution of acetonitrile in the formation of this atomic arrangement via a parallel and antiparallel alignment of the molecules among first neighbors

and radial orientation in the coordination of Li⁺. Figure 2b,c shows the influence of the cosolvents on the position and width of the peaks assigned to the intermediate-range atomic ordering as extracted from the fits. These parameters are presented as functions of the cosolvents' dielectric constants, ε , and are inversely related to the size of the repetition units within the atomic arrangement and their ordering degree, respectively. In Figure 2 and the subsequent data presentation along with the manuscript, a value of $\varepsilon = 1$ has been assigned to the cosolvent-free solution. Together, the results in Figure 2c,d were used to estimate the size of the probed atomic ordering with Scherrer's formula $L = \frac{0.9\lambda}{B\cos\theta}$, where L is the size of the atomic ordering, 0.9 is a dimensionless shape factor (considering a spherical shape of the correlated region), λ is the wavelength of the X-ray beam, B is the broadening of the Bragg reflection, and θ is the scattering angle. The sizes of the atomic orderings are presented in Figure 2d and primarily allow for a qualitative discussion, while the quantitative estimates must be considered with caution for small structural dimensions, as explained in ref 64. Here, the most relevant differences are associated with the addition of water to the solution, which leads to a shorter intermediate-atomic ordering.

The radial distribution functions (RDF) obtained via MD (Figure 3) provide good complementary insight into the structure of the solutions. Note that the RDFs simulated for the cosolvent-free solution and the one cosolvated with acetone are replicated from ref 19. The WAXS data in Figure 2d show that adding toluene or dichloromethane may slightly reduce the size of the intermediate-range atomic ordering and, as recognized from the RDF in Figure 3a (for the peak at ~0.35 nm), alters the acetonitrile population in the cations' first solvation sheath. Here, the RDF shows a change in the intensity of its peaks but not in their areas, indicating that a narrower distribution of Li⁺—acetonitrile interactions is obtained but these do not become more abundant in comparison with the cosolvent-free system. In addition, neither

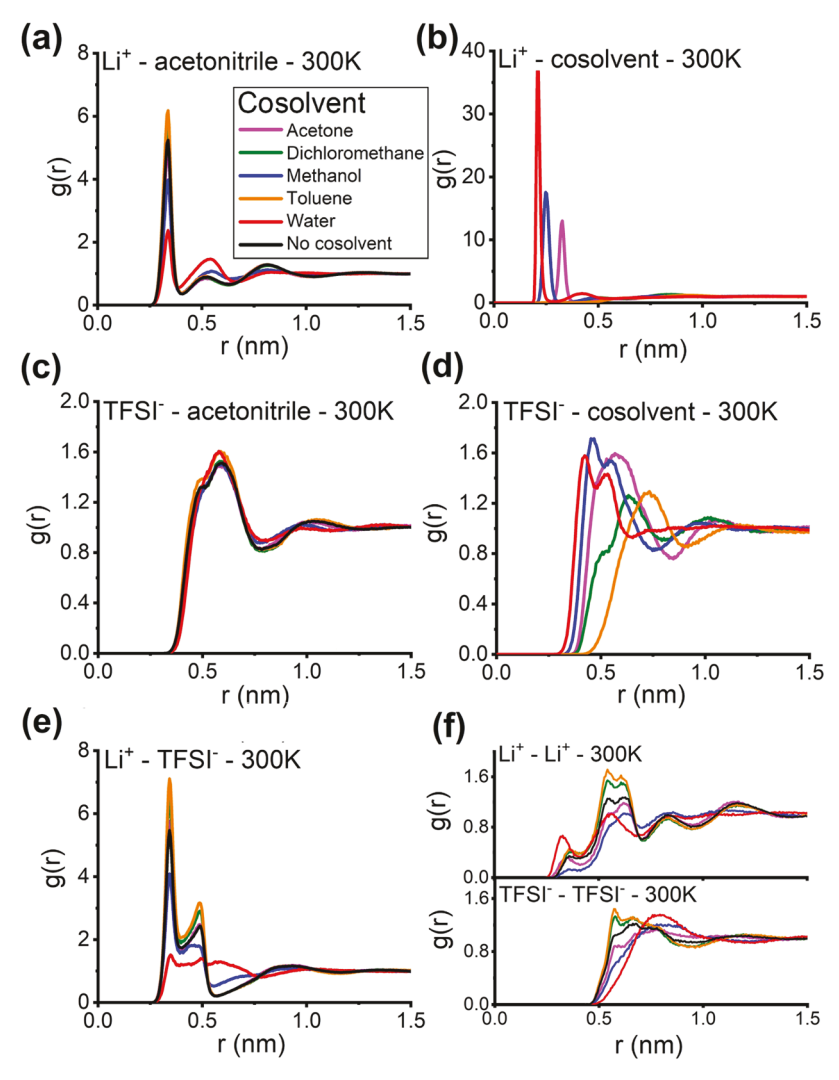


Figure 3. RDF curves for the different interactions within the acetonitrile/LiTFSI solutions (3:1 molar ratio) with different cosolvents. The legend in (a) stands for the whole figure. (a) Li⁺—acetonitrile interactions. The curves from the solutions cosolvated with toluene (orange) and dichloromethane (green) are superposed as well as those from the cosolvent-free solution (black) and that with acetone (pink). (b) Li⁺—cosolvent interactions. The curves from the solutions cosolvated with toluene (orange) and dichloromethane (green) are not visible in the presented scale. (c) TFSI⁻—acetonitrile interactions. Most of the curves are nearly superposed. (d) TFSI⁻—cosolvent interactions. (e) Li⁺—TFSI⁻ interactions. The curves from the solutions cosolvated with toluene (orange) and dichloromethane (green) are superposed, as well as those from the cosolvent-free solution (black) and that with acetone (pink). (f) Li⁺—Li⁺ (top) and TFSI⁻—TFSI⁻ (bottom) interactions. The curves from the solution with no cosolvent are reproduced from ref 19. Figure 1: (a) Temperature-dependent conductivity measurements of acetonitrile/LiTFSI solutions (3:1 molar ratio) with different cosolvents; (b) Walden plot of acetonitrile/LiTFSI solutions with different cosolvents; the red dashed line refers to the ideal case corresponding to a dilute aqueous solution.

toluene nor dichloromethane engages in cations coordination (Figure 3b).

As revealed by the WAXS data, the dimension of the intermediate-range atomic ordering is not altered by the addition of acetone and methanol. As discussed in ref 20, the addition of acetone leads to the incorporation of the cosolvent into the Li⁺ solvation sheath but without fully releasing acetonitrile as "free" molecules. With methanol, a more prominent substitution of acetonitrile by the cosolvent in the solvation of Li⁺ occurs, as exposed in Figure 3a. Meanwhile, the RDFs also show that the shorter intermediate-range ordering formed upon the addition of water is accompanied by an efficient replacement of acetonitrile by the cosolvent in the coordination of the cations (see Figure 3a,b).

Differently from the situation for cations, the TFSI-acetonitrile RDF is not drastically affected by any of the

cosolvents (Figure 3c). In principle, the peaks in Figure 3c are related to the characteristic coordination of the anion's S=O groups by acetonitrile's CH3 termination.65 However, the distances between the peaks and the subsequent minima exceed the sum of the van der Waals radii from the anion's atoms and the acetonitrile's methyl group, not allowing for the consideration of prevalent direct TFSI-acetonitrile coordination. Following the same rationale, direct interactions between TFSI- and the cosolvents are also not likely, as shown in Figure 3d. The cosolvents with the highest dielectric constants, water and methanol, present populations around the anions, possibly related to interactions involving TFSI-'s O and S atoms, 65 but at distances larger than those expected for direct coordination. As shown in Figure S5 (SI), however, our IR experiments do show that the vibrations from the S=O bonds in TFSI are sensitive to the addition of these

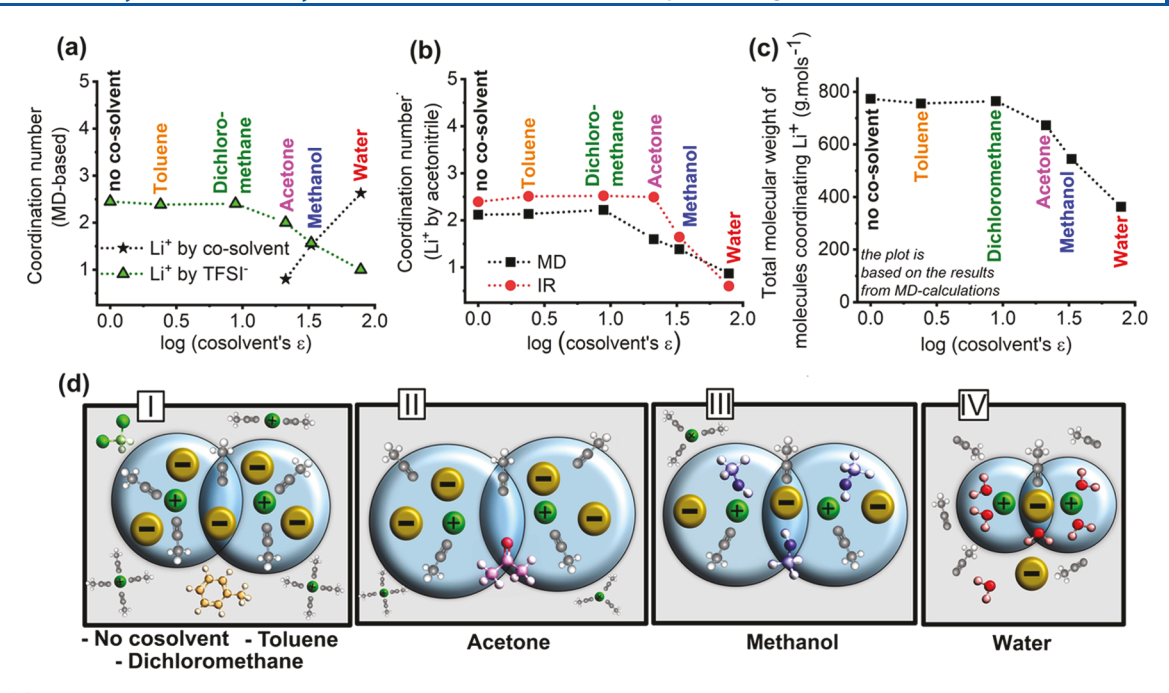


Figure 4. (a) Coordination numbers determined via molecular dynamics simulations of Li⁺ by the cosolvents and of Li⁺ by TFSI⁻. The Li⁺-TFSI⁻ coordination was determined for the water-containing system despite the disordered character of these interactions, as explained in the text. (b) Coordination numbers of Li⁺ by acetonitrile determined by molecular dynamics simulations (MD) and infrared (IR) spectroscopy experiments. (c) Sum of the molecular weights from the molecules of acetonitrile, cosolvents, and TFSI⁻ coordinating the Li⁺. (d) Illustration of the solvation structures based on the coordination numbers determined via MD and IR (Li⁺ by acetonitrile) for the solutions with the different cosolvents.

cosolvents. Likewise, toluene and dichloromethane interact with the anion's C-F groups (see Figure S5)⁶⁵ but not via direct coordination.

The cation-anion interactions are not drastically altered by acetone in comparison with the cosolvent-free solution (Figure 3e). For the cases of toluene and dichloromethane, the increase in the intensities of the RDF peaks could, in principle, suggest an increase in the populations of anions around the cations. However, as also discussed for the Li⁺-acetonitrile interactions, the areas of the peaks are not significantly altered, indicating that the TFSI⁻ population around the Li⁺ becomes less dispersed but not more abundant. Contrarily, the addition of methanol inhibits the Li⁺-TFSI⁻ short-range interactions and partially shifts these from close contact (~0.35 nm) to solvated pairs (0.6 nm). This effect is even more pronounced in the presence of water, which drives the formation of a highly disordered distribution of anions around the cations. As shown in Figure S5, the IR experiments corroborate the simulations as they indicate a disturbance in the cation-anion coordination with the addition of water via the redshift of the vibrations from TFSI-'s S-N-S bonds.66 Regarding the cation-cation interactions (Figure 3f, top), these are promoted by water in the short range and by toluene and dichloromethane in the longer range. These interactions are also diminished by the addition of methanol and not considerably altered by acetone. As for the anion-anion interactions (Figure 3f, bottom), these do not occur as close contact in any of the cases but are promoted by toluene and dichloromethane, impeded by acetone and especially methanol, and shifted to even longer distances by water.

Coordination Structure: Molecular Dynamics and Infrared Spectroscopy. To understand the short-range, or coordination structures within the solutions, coordination numbers at room temperature were obtained from the integrated areas below the first peaks of the RDFs (details in

Section S1) and are presented in Figure 4 as functions of the cosolvents' ε . Graphical representations of the predominant solvation structures conceived based on the data presented in Figure 4a-c, are displayed in Figure 4d. These illustrations are intended to represent the more likely, but not the only possible solvation complexes in the solutions, and are charge-balanced by smaller solvation complexes and/or uncoordinated anions. In Figure 4a, the coordination numbers of the cation by the cosolvents and TFSI⁻ (interacting molecules per Li⁺ unit) are presented. The coordination numbers of Li⁺ by toluene and dichloromethane were not determined due to the absence of well-defined minima after the first RDF peaks (which suggests a scarcity of cosolvent molecules in Li⁺ coordination). Similarly, the RDF describing the Li⁺-TFSI⁻ interactions for the case of water as cosolvent does not present a clear definition of the first peaks because of the disordered nature of the interactions. Hence, a coordination number of Li⁺ by water was estimated by integrating the area under the RDF curve until g(r) = 0.52 nm, where the end of a peak-like feature is observed (note that following this procedure to determine the coordination of Li⁺ by toluene and dichloromethane led to very low coordination numbers ~0.1). Toluene and dichloromethane do not change considerably the Li⁺-TFSI⁻ coordination in comparison with the cosolvent-free solution. In all of these cases, we determined that ~2.4 molecules of TFSI⁻ participate in the solvation of Li⁺, which is somewhat in line with the value reported by Kameda et al.⁶⁷ These authors used neutron diffraction measurements and determined that Li⁺ is coordinated by ~2 molecules of TFSI⁻ in a cosolventfree solution with acetonitrile/LiTFSI $\approx 3:1$. Also, the results in Figure 4a reinforce a larger population of water molecules around the cations compared with the other cosolvents.

In Figure 4b, the MD-determined coordination numbers of Li⁺ by acetonitrile are compared with their counterparts determined experimentally with IR spectroscopy (details in

Section S1). In comparison with the MD-based coordination numbers, the values obtained with IR are expected to be higher, since they account for the content of acetonitrile molecules that are under influence of the cations, regardless of the solvent being at the first or outer solvation sheaths. For the cases with toluene, dichloromethane, and methanol, the IRbased coordination numbers are less than 20% higher than those obtained via MD. In contrast, this difference is higher than 55% for the solution with acetone, indicating that the molecules of acetonitrile are considerably influenced by the cations beyond the first solvation sheath as discussed in ref 19. For the solution with water, the IR-based coordination number of Li⁺ by acetonitrile is slightly lower than the MD-based result, indicating that the replacement of the main solvent by the cosolvent might be even more drastic than predicted by the calculations and that the influence of the cations over molecules of acetonitrile beyond the first solvation sheath is minimal. Likewise observed for the Li⁺-TFSI⁻ coordination, toluene, and dichloromethane do not significantly change the Li⁺-acetonitrile coordination compared with the cosolventfree solution. In these cases, ~2.1 molecules of acetonitrile (as determined by MD) are involved in the solvation of each cation, while Kameda et al., report a coordination of ~1.7 molecules of the solvent per Li^{+.6767} In Figure 4c, the sum of the molecular weights of the molecules of acetonitrile, cosolvents, and TFSI- coordinating the cations (based on the MD-determined coordination numbers) is displayed and the reader can appreciate how the solvation structures promoted by water are lighter in comparison with the other cosolvents. As summarized in Figure 4d, toluene and dichloromethane barely change the coordination structure found in the cosolvent-free solution (Figure 4d-I), and acetone induces the formation of large complexes with considerable presence of acetonitrile and TFSI⁻ (Figure 4d-II). Such an effect is reduced with methanol (Figure 4d-III) as well as the Li⁺-TFSI⁻ close-contact interactions, which become less ordered and are partially shifted to longer distances. Water leads to small complexes and aggravates the effects on the Li⁺-TFSI interactions observed in the methanol-containing solution (Figure 4d-IV).

Dynamics in the Solutions: QENS and MD. While presenting the QENS experiments, the indexes p- and d- stand for the protiated and deuterated solvents, respectively. Primarily, for the analysis of the dynamics within the electrolytes, QENS experiments were performed at 260, 280, and 300 K and combined with MD. Additional QENS data were collected at 20 K and these data were initially intended to be used as the instrumental resolution as conventional diffusive and rotational motions in the electrolytes are expected to be inactive at such cryogenic temperature. As discussed in the SI (Figure S14), however, all samples containing p-acetonitrile and d-cosolvents presented detectable QENS signals. This feature has been reported in QENS measurements with ionic liquids that form crystalline structures upon cooling and is associated with methyl rotation tunneling, which is facilitated by the addition of LiTFSI. 68,69 In our case, although broad distributions of tunneling peaks are observed, they show that all of the solutions retain the characteristics of the original cosolvent-free electrolyte.

Turning to the analysis of the solutions' dynamics, Figure 5a displays the ions' diffusion coefficients, $D_{\rm Li}$ and $D_{\rm TFSI}$, at 300 K as determined with MD and these values are listed in Table 2. The coefficients for the sample with no cosolvent are

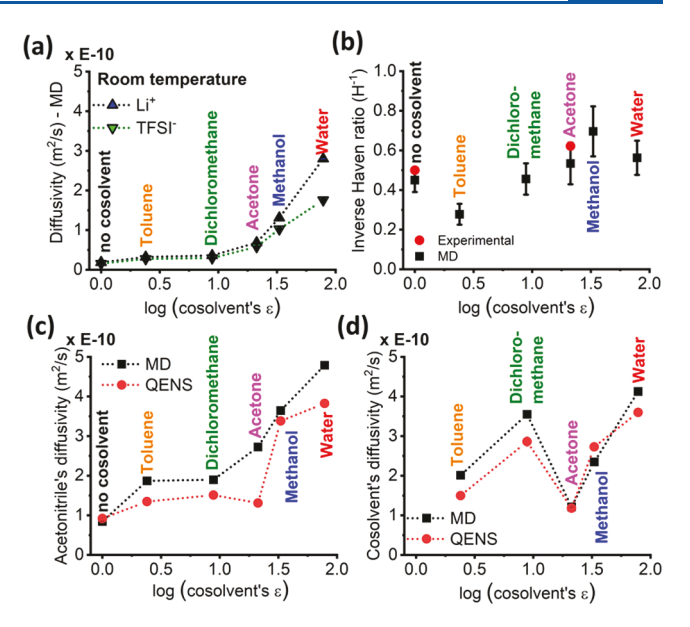


Figure 5. (a) Diffusion coefficients of Li⁺ and TFSI⁻ as obtained via MD at room temperature for electrolytes containing different cosolvents. (b) Ratios between the Einstein–Helfand ($\sigma_{\rm EH}$) and Nernst–Einstein ($\sigma_{\rm NE}$) conductivities. Red dots are experimental data extracted from refs 19 and 31. (c) Diffusivities of p-acetonitrile as obtained via MD (black) and QENS (red) for electrolytes containing different d-cosolvents. (d) Diffusivities of the different p-cosolvents as obtained via MD (black) and QENS (red).

reproduced from ref 19. In the solutions with toluene and dichloromethane, D_{Li} and D_{TFSI} are very similar to each other and slightly higher than in the absence of cosolvents. Upon the addition of acetone, D_{Li} and D_{TFSI} slightly increase but remain similar to each other, whereas methanol increases the ionic mobility with a higher value of D_{Li} compared with D_{TFSI} . In the water-containing solution, the ions are further accelerated and the discrepancy between D_{Li} and D_{TFSI} is more noticeable. The temperature dependences of D_{Li} and D_{TFSI} are displayed in Figure S6, where one can recognize that at all experimental temperatures, they present the same trend shown in Figure 5a. Also in Figure S6, the activation energies of $D_{\rm Li}$ and $D_{\rm TFSI}$ as obtained with the interpolations with the Arrhenius equation are displayed. For the cases with no cosolvent, water, acetone, and methanol, the activation energies of the ionic motions are comparable and have an average value of ~6 kcal/mol, whereas in the solutions with toluene, and dichloromethane this value increases to ~8 kcal/mol. We note here that these values are higher than those determined elsewhere for even more concentrated LiTFSI/acetonitrile solutions in which Li+ hoping has been considered the main mechanism of ionic transport, and the corresponding activation energy was reported to be ~3 kcal/mol.³⁴

The conductivities of the solutions at 298 K were calculated with MD using the Nernst–Einstein and Einstein–Helfand equations, $\sigma_{\rm NE}$ and $\sigma_{\rm EH}$. As shown in eq 1, $\sigma_{\rm NE}$ solely considers the ionic diffusivities and concentrations while $\sigma_{\rm EH}$ also accounts for the translational dipole moments of the solvents and provides better approximation with experimental results, as shown in Figure S7.

Table 3. Diffusion Coefficients Obtained for Different Chemical Species via Different Methods

cosolvent	$D_{ m Li}~({ m MD})$	D_{TFSI} (MD)	$D_{ m acetonitrile}~({ m MD})$	$D_{ m cosolvent}$ (MD)	$D_{ m acetonitrile}$ (QENS)	$D_{\mathrm{cosolvent}}$ (QENS)		
no cosolvent	0.186 ± 0.005	0.154 ± 0.005	0.844 ± 0.012		0.920 ± 0.013			
toluene	0.324 ± 0.018	0.284 ± 0.012	1.861 ± 0.021	2.014 ± 0.039	1.345 ± 0.016	1.499 ± 0.068		
dichloromethane	0.389 ± 0.028	0.332 ± 0.027	1.987 ± 0.030	3.829 ± 0.134	1.510 ± 0.019	2.861 ± 0.132		
acetone	0.700 ± 0.020	0.622 ± 0.025	2.631 ± 0.078	1.351 ± 0.020	1.310 ± 0.080	1.180 ± 0.010		
methanol	1.270 ± 0.043	1.065 ± 0.034	3.823 ± 0.055	2.397 ± 0.078	3.382 ± 0.042	2.728 ± 0.032		
water	2.690 ± 0.052	1.720 ± 0.042	4.601 ± 0.064	3.946 ± 0.061	3.825 ± 0.029	3.598 ± 0.031		
^a All values are presented in 10^{-10} m ² /s.								

$$\begin{split} \sigma_{\rm NE} &= \frac{q^2}{k_{\rm B}T} (n_{\! +} D_{\rm Li} \, + \, n_{\! -} D_{\rm TFSI}) \\ \sigma_{\rm EH} &= \frac{1}{6V k_{\rm B}T} \lim_{t \to \infty} \frac{\rm d}{\rm d} \langle [\overrightarrow{M_{\rm J}}(t) \, - \, \overrightarrow{M_{\rm J}}(0)]^2 \rangle; \ \overrightarrow{M_{\rm J}}(t) \\ &= \sum_i q_i \overrightarrow{r_i}(t) \\ H^{-1} &= \frac{\sigma_{\rm EH}}{\sigma_{\rm NE}} \end{split} \label{eq:sigma_loss}$$

where $k_{\rm B}$ is the Boltzmann constant, q is the elementary charge, n_{+} and n_{-} are the corresponding ionic concentrations of cations and ions, $\overrightarrow{M_{\rm I}}(t)$ are the translational dipole moments, and $\vec{r}_i(t)$ and q_i are the center-of-mass coordinate and charge for ion i, respectively. Then, as displayed in Figure 5b, the ratios between σ_{EH} and σ_{NE} were obtained and these are known in the literature as the inverse Haven ratio (H^{-1}) , which provides us with a measure of the strength of ion-ion correlations that negatively affect the conductivity. For reference purposes, the values of H^{-1} determined experimentally in previous works for the cosolvent-free²¹ and the acetone-containing²⁰ solutions are also displayed. For the solutions with dichloromethane, acetone, methanol, and water, H^{-1} is comparable with the cosolvent-free system, whereas the addition of toluene leads to a detectable increase in the ionic correlations' strength (or a decrease in H^{-1}).

For the diffusivities of acetonitrile and the cosolvents, Figure 5c,d, the MD simulations were benchmarked by the experimental QENS results. The results obtained with both MD and QENS are listed in Table 3. These figures contain the results obtained at 300 K, while those obtained at 260 and 280 K are displayed in Figure S8. The respective activation energies are also displayed in Figure S7 and vary between 6 and 7 kcal/mol, with no remarkable differences between all of the samples. For the analyses of the QENS data, the measured signals, I(Q, E), were described as

$$I(Q, E) = [x(Q)\delta(E) + (1 - x(Q))S(Q, E)]$$

$$\otimes R(Q, E) + B(Q, E)$$
(2)

where x(Q) is the fraction of elastic scattering (zero energy transfer) arising from molecules that are either immobilized or are slower than the instrument resolution timescale (longer than \sim 0.36 ns), $\delta(E)$ is a Dirac δ function that accounts for the elastic scattering, S(Q, E) is the model-dependent dynamic scattering function, B(Q, E) is a linear temperature- and sample-dependent background, and R(Q, E) is the instrument resolution function. Since in the temperature range explored in the present work we may expect that all molecules in the fluid perform detectable motions, no elastic contributions were

considered, *i.e.*, x(Q) = 0. The dynamic structure factor was fitted in most cases with a stretched Cole—Cole distribution

$$S(Q, E) = \left(\frac{1}{\pi\Gamma(Q)}\right) \times \left[\frac{\left(\frac{E}{\Gamma(Q)}\right)^{-\alpha}\cos\left(\frac{\pi\alpha}{2}\right)}{1 + 2\left(\frac{E}{\Gamma(Q)}\right)^{1-\alpha}\sin\left(\frac{\pi\alpha}{2}\right) + \left(\frac{E}{\Gamma(Q)}\right)^{2(1-\alpha)}}\right]$$
(3)

where $\Gamma(Q)$ corresponds to the half-width at half-maximum of the signal and α is a stretching factor ($0 \le \alpha \le 1$). The only exception is the sample with d-acetonitrile/p-toluene/LiTFSI, to which eq 3 did not describe the data well, as described in detail in the SI (Figure S11). For this sample, a model with two Lorentzian functions was used, and the presence of a fast and a slow component was considered. To obtain the diffusion coefficients, the Q^2 -dependences of $\Gamma(Q)$ were fitted with the jump-diffusion model (the fits are shown in Figures S9 and S10)

$$\Gamma(Q) = \frac{\hbar D Q^2}{1 + D Q^2 \tau_0} \tag{4}$$

where τ_0 is the residence time between jumps. In most cases, $\Gamma(Q)$ could be fitted considering $\tau_0 = 0$, and eq 4 was reduced to a continuous diffusion equation.

In Figure 5c,d, the diffusivities determined by QENS and MD for acetonitrile and the cosolvents follow the same trends with the change in permittivity, and the differences between experiments and simulations are explained below. In Figure 5c, $D_{\text{acetonitrile}}$ has a comparable behavior to the ionic diffusivities, as it goes along with the solutions' viscosities (Figure 1b), inversely correlates with the dimensions of the intermediaterange ordering (Figure 2d), and agrees with the evolution of the Li⁺-acetonitrile coordination (Figure 4). As such, the higher values of $D_{\text{acetonitrile}}$ upon the addition of water and methanol highlight the occurrence of solvent exchange in the ionic coordination and, consequently, the release of "free" molecules of acetonitrile to the solution. As presented in Figure S12, this trend is directly reflected in the raw QENS data and is, therefore, model-independent, and the differences between the MD and QENS results are likely due to an overestimation of the contributions from free molecules of acetonitrile and small Li+-acetonitrile complexes in the simulations. In any case, the values of $D_{\text{acetonitrile}}$ obtained by either QENS or MD are considerably lower than the values estimated elsewhere for neat acetonitrile (\sim 40 \times 10⁻¹⁰ m²/ $s).^{71}$

Differently from acetonitrile, the differences between the QENS data from the cosolvents are not directly detectable in the raw experimental data (see Figure S12). Hence, the outcomes of the data analysis are more dependent on the model used to describe S(Q, E) but good agreements with the MD results are still obtained, as shown in Figure 5d. Here, although water strongly engages in ionic coordination, the resulting solvation complexes are small and light enough to allow for the fast motions determined for the cosolvent. For toluene, since the QENS data was described by a twocomponent model, D_{toluene} in Figure 5d refers to the slow component. Given the very low dielectric constant, a more pronounced microscopic phase separation due to the presence of weakly interacting molecules of toluene is expected and justifies the need of using two independent dynamic components in the QENS data. For the fast component, $D_{\text{toluene-fast}}$ was determined as $\sim (22 \pm 5) \times 10^{-10} \text{ m}^2/\text{s}$ at 300 K (Figure S10), which is nearly half of the value determined elsewhere with NMR for the neat solvent.7

DISCUSSION

According to our results, the changes in conductivity in the LiTFSI/acetonitrile solution driven by different cosolvents cannot be solely explained by the changes in viscosities and the ionic mobilities in the systems. The effects driven by each of the cosolvents are different and ought to be individually discussed. Hence, we focus on two interesting comparisons: (i) between the cosolvent-free solution and the solutions containing toluene and dichloromethane and (ii) between the solutions with acetone, methanol, and water. Regarding the first comparison, neither toluene nor dichloromethane is fully inert in the solutions as one could assume based on the low dielectric constants. Although these cosolvents do not engage in direct ionic coordination, they disturb the vibrational bands of the nonpolar CF3 groups in the TFSI-'s molecules, as revealed by our IR experiments. Still, the QENS analysis suggests that a fraction of the cosolvents with low dielectric constants is less involved in the overall interactions within the system. In the particular case of the toluene-containing solution, the diffusive dynamics of the cosolvent could only be reasonably described with a two-component model. For this case, the diffusivity associated with a faster fraction of toluene is only lower by a factor of \sim 2 in comparison with the neat compound while the viscosity of the cosolvated solution is higher by a factor of ~18. Even though this is a modeldependent outcome, it suggests the existence of microscopic phase separation within the solution in which a fraction of the cosolvents with low dielectric constants are less influenced by the ions and perform more independent motions.

At room temperature, in comparison with the cosolvent-free solution, toluene and dichloromethane reduce the solution's conductivity although the viscosity decreases, and the overall mobilities of solvents and ions increase. In several works, the mechanisms reported to explain unusual conductivities in concentrated systems are highly dependent on the coordination of the cations. For example, Li⁺ hopping mechanisms have been associated with the transit of Li⁺ toward sites previously occupied by the cations themselves, with critical participation of coordinating anions and solvents. ^{32,34,35} Here, however, both toluene and dichloromethane do not promote relevant changes in the coordination numbers of Li⁺, either by TFSI⁻ or acetonitrile (Figure 4), but, in comparison with the cosolvent-free solution, these cosolvents slightly narrow the distributions

of anions and acetonitrile in the solvation sheath of the cations (Figure 3e). Then, the abundant Li+-TFSI- close-contact interactions in these systems promote the existence of ion pairs that diffuse together but with zero net charge movement and thus no contribution to conductivity. Such an effect is enhanced upon the addition of toluene as this sample combines similar values of D_{Li} and D_{TFSD} a lower value of H^{-1} , and slightly higher activation energies for ionic motions. The anion-solvent interactions have also been proven to be determinant for the decoupling between conductivity and viscosity in concentrated solutions via, for example, percolation mechanisms.^{31,33} They are not critical in the solutions containing toluene and dichloromethane since, as indicated by MD, the TFSI-acetonitrile interactions remain fairly unaltered. The interactions between TFSI⁻ and the cosolvents are potentially more critical in the solutions cosolvated with water and methanol, as described in the sequence. Finally, our results obtained for the solutions containing toluene and dichloromethane indicate an increase of both the anion-anion and cation-cation interactions in comparison with the cosolvent-free solution (Figure 3f). However, these are promoted at fairly long distances and do not indicate the occurrence of correlated motions that could positively influence conductivity.

Now we turn to the comparison between the solutions cosolvated with acetone, methanol, and water, which, in contrast to the solutions containing toluene and dichloromethane, present more drastic alterations in the coordination arrangements, as follows. According to the IR results, acetone engages in the coordination of the cations but without releasing acetonitrile as free molecules. Here, we highlight that the content of acetonitrile molecules under influence of the cations is underestimated by the simulations (Figure 4b), which, in turn, overestimates the average diffusivity of this solvent (Figure 5c). This effect has also been observed and discussed in detail in our previous publication¹⁹ and is a consequence of the comparable dipole moments of acetonitrile and acetone. While the latter engages in the solvation of Li+, it does so without efficiently screening the cations and thus allowing molecules of acetonitrile to form an extended solvation shell. Although such an effect is more critical for the experiments in the present work, it is well captured by the simulations when solutions with larger contents of acetone are investigated.¹⁹ Also, the addition of acetone changes the coordination number of Li+ by TFSI- from 2.5 (in the cosolvent-free solution) to 2. Meanwhile, methanol promotes a more prominent solvent exchange in the coordination of the cations and impairs the Li+-TFSI- close-contact interactions by reducing the coordination number of Li⁺ by TFSI⁻ to 1.5 and water further intensifies such effects. At a first glance, one could argue that water and methanol promote ionic mobility via mechanisms that resemble a simple dilution process: (i) the viscosity decreases as an inherent consequence of the reduction in ionic concentration upon cosolvation; (ii) the ionic screening improves due to the cosolvents' high dielectric constants;⁷³ (iii) in the water-containing solution, the intermediate-range atomic ordering in the cations' solvation is highly packed and light, thus allowing for rapid motions of Li⁺; and (iv) acetonitrile molecules are released from the ionic coordination, which improves the overall mobility in the solution. Nevertheless, some relevant outcomes cannot be fully interpreted as a simple dilution. First, by comparing the samples with acetone and methanol, the latter presents lower

viscosity and higher mobility of ions and solvents but with no benefits to conductivity. In additionality, Popov et al. 31 have previously determined $H^{-1} \sim 0.75$ for a water/LiTFSI solution (1:3 molar ratio), whereas our estimation for the water/ acetonitrile/LiTFSI solution points to a comparable value despite the lower salt concentration (4.2:1 solvents/salt molar ratio). As such, the room-temperature conductivity reported by Popov et al. for the water/LiTFSI solution is nearly 2-fold higher than for our cosolvated water/acetonitrile/LiTFSI system, which is, in turn, more than 5 times less viscous. From our results, we hypothesize that the interactions between the cosolvents and TFSI- play a very important role in these discrepancies. As shown in Figure 5a, while the cosolvation with methanol and water does improve the ionic mobility, such an effect is less pronounced for TFSI-, which becomes slower than Li⁺ in the solutions with those cosolvents, even if the proposed solvation structures around the cations are much larger than a single TFSI molecule (Figure 4d). Also, as revealed by the RDFs in Figure 3d, as the dielectric constant of the cosolvent molecules increases, they approach the TFSImolecules. Indeed, even though the populations of methanol and water are located at somewhat long distances from the anions, these can disturb the vibrational behavior of TFSI, as revealed by IR (Figure S5). To a certain extent, the distinct influence of methanol and water over the molecules of TFSI, compared with the effect of acetone can also be appreciated in the WAXS experiments. In these, the Bragg reflections assigned to the internal structure factor of the anions are broader in the presence of acetone (see Figure S4). Once more referring to the work by Popov et al., 31 the authors have comprehensively described the influence of the strong interactions between TFSI- and solvent molecules (water and acetonitrile) as a critical factor in the reduced conductivities in comparison with similar solutions of lithium bis(fluorosulfonyl)imide (LiFSI). In such a case, the authors highlight that the consequent lower mobility of solvent molecules is directly associated with lower conductivities. In the present work, it is also possible to highlight how the anions/cosolvent interactions influence the Li+-Li+ and TFSI-TFSI interactions and potentially affect the conductivities, especially in the water-containing solution. From the RDFs presented in Figure 3f, water promotes an increase in close-contact Li⁺-Li⁺ interactions, which indicates the occurrence of collective dynamics of cations that could, in principle, benefit conductivity. Nevertheless, an opposite effect occurs for the anions, and only long-range TFSI-TFSIinteractions are promoted.

CONCLUSIONS

Combining various experimental and simulation results, we report a comprehensive analysis of the physicochemical factors controlling the conductivities of acetonitrile/LiTFSI solution cosolvated with liquids with different dielectric constants. In all cases, the resulting solutions exhibit features resembling the original (undiluted) electrolyte, and the cosolvation-induced effects cannot be ascribed to simple dilution processes. The present work revealed that among these specific features, there is, for example, an intermediate-range atomic ordering whose origin is based on both ion—ion and solvent-ion interactions. Also, and most importantly, the cosolvated solutions present abundant ion—ion correlations, which are correspondingly expected in concentrated systems. The strength of these correlations does not seem to be altered upon the addition of the different cosolvents, except in the case of toluene, which

seemingly enhances such correlations. When cosolvents with low dielectric constants (toluene and dichloromethane) are added, the room-temperature conductivity decreases despite the decrease in viscosities and increase in ionic mobilities. Such an effect is related to the populations of TFSI around Li+, which are equally abundant but become more ordered upon the addition of those cosolvents. Inversely, the addition of cosolvents with high dielectric constant, such as methanol and water, promotes a disordered character to the Li⁺-TFSI⁻ interactions and a prominent solvent exchange in the cations' solvation. Still, the conductivities of the resulting solutions are not as high as one could expect in a simple dilution mechanism due to strong interactions between the cosolvents and TFSI-. Finally, as we perform the cosolvation with acetone, whose dielectric constant is moderate compared with acetonitrile, intermediary mechanisms are triggered. For this case, most of the features associated with ion-ion and ion-solvent interactions are comparable with the cosolvent-free solution even if acetone molecules are incorporated into the cations' solvation. From our results, one could, in principle, expect that systems containing different solvents and cosolvents with similar ratios of dielectric constants should present similar behaviors. However, it has been shown that local solvation effects, such as the formation of hydrogen bonds, may affect dipole moments of solvents in solutions²⁸ and, therefore, their interactions with ions. The possibility that different systems may exhibit some other interesting individualities will be scrutinized in our future investigations.

ASSOCIATED CONTENT

Supporting Information

The Supporting Information is available free of charge at https://pubs.acs.org/doi/10.1021/acs.jpcb.2c07327.

Additional experimental details and supporting results from MD, conductivity, IR, and OENS (PDF)

AUTHOR INFORMATION

Corresponding Authors

Murillo L. Martins — Department of Chemistry, University of Tennessee, Knoxville, Tennessee 37996, United States;
orcid.org/0000-0002-3883-9114; Email: mmart201@utk.edu

Eugene Mamontov — Neutron Scattering Division, Oak Ridge National Laboratory, Oak Ridge, Tennessee 37831, United States; orcid.org/0000-0002-5684-2675; Email: mamontove@ornl.gov

Authors

Xiaobo Lin – Department of Chemical and Biomolecular Engineering, Vanderbilt University, Nashville, Tennessee 37235, United States

Catalin Gainaru — Chemical Sciences Division, Oak Ridge National Laboratory, Oak Ridge, Tennessee 37831, United States

Jong K. Keum – Neutron Scattering Division, Oak Ridge National Laboratory, Oak Ridge, Tennessee 37831, United States; Center for Nanophase Materials Sciences, Oak Ridge, Tennessee 37831, United States

Peter T. Cummings – Department of Chemical and Biomolecular Engineering, Vanderbilt University, Nashville, Tennessee 37235, United States Alexei P. Sokolov — Department of Chemistry, University of Tennessee, Knoxville, Tennessee 37996, United States; Chemical Sciences Division, Oak Ridge National Laboratory, Oak Ridge, Tennessee 37831, United States; ocid.org/ 0000-0002-8187-9445

Robert L. Sacci — Chemical Sciences Division, Oak Ridge National Laboratory, Oak Ridge, Tennessee 37831, United States; © orcid.org/0000-0002-0073-5221

Complete contact information is available at: https://pubs.acs.org/10.1021/acs.jpcb.2c07327

Author Contributions

M.L.M. performed the QENS experiments and data analysis together with E.M., prepared the samples, performed IR experiments and data analysis, analyzed the data from molecular dynamics simulations, performed conductivity experiments and WAXS, and wrote the paper. X.L. performed the molecular dynamics calculations with support from P.T.C. C.G. performed the conductivity measurements with support from A.P.S. R.L.S. provided support for the IR and viscosity experiments and sample preparation. All authors proofread the text and provided input to the discussions in the whole manuscript.

Notes

The authors declare no competing financial interest.

ACKNOWLEDGMENTS

This research used resources at the Spallation Neutron Source and Center for Nanophase Materials Sciences, DOE Office of Science User Facilities operated by the Oak Ridge National Laboratory (ORNL). This work was supported as part of the Fluid Interface Reactions, Structures and Transport (FIRST) Center, an Energy Frontier Research Center funded by the U.S. Department of Energy, Office of Science, Office of Basic Energy Sciences. This research used resources of the National Energy Research Scientific Computing Center (NERSC), a DOE Office of Science User Facility supported by the Office of Science of the U.S. Department of Energy under Contract No. DE-AC0205CH11231. ORNL is managed by UT-Battelle, LLC, for U.S. DOE under Contract No. DEAC05-00OR22725. M.L.M. acknowledges partial support from NSF (award CHE-2102425) for writing the manuscript and part of the data analysis. J.K.K. acknowledges the ORNL instrumentation pool and ORNL Laboratory Directed Research and Development for the use of Xeuss 3.0 SAXS/WAXS. The authors are also thankful to Dr. Luke Daemen for providing chemical reagents for the neutron scattering experiments.

REFERENCES

- (1) Suo, L.; Hu, Y.-S.; Li, H.; Armand, M.; Chen, L. A New Class of Solvent-in-Salt Electrolyte for High-Energy Rechargeable Metallic Lithium Batteries. *Nat. Commun.* **2013**, *4*, No. 1481.
- (2) Messaggi, F.; Ruggeri, I.; Genovese, D.; Zaccheroni, N.; Arbizzani, C.; Soavi, F. Oxygen Redox Reaction in Lithium-Based Electrolytes: From Salt-in-Solvent to Solvent-in-Salt. *Electrochim. Acta* 2017, 245, 296–302.
- (3) Borodin, O.; Suo, L.; Gobet, M.; Ren, X.; Wang, F.; Faraone, A.; Peng, J.; Olguin, M.; Schroeder, M.; Ding, M. S.; Gobrogge, E.; von Wald Cresce, A.; Munoz, S.; Dura, J. A.; Greenbaum, S.; Wang, C.; Xu, K. Liquid Structure with Nano-Heterogeneity Promotes Cationic Transport in Concentrated Electrolytes. *ACS Nano* **2017**, *11*, 10462—10471.

- (4) Seo, D. M.; Borodin, O.; Han, S.-D.; Boyle, P. D.; Henderson, W. A. Electrolyte Solvation and Ionic Association II. Acetonitrile-Lithium Salt Mixtures: Highly Dissociated Salts. *J. Electrochem. Soc.* **2012**, *159*, A1489—A1500.
- (5) Mandai, T.; Yoshida, K.; Ueno, K.; Dokko, K.; Watanabe, M. Criteria for Solvate Ionic Liquids. *Phys. Chem. Chem. Phys.* **2014**, *16*, 8761.
- (6) Yoshida, K.; Nakamura, M.; Kazue, Y.; Tachikawa, N.; Tsuzuki, S.; Seki, S.; Dokko, K.; Watanabe, M. Oxidative-Stability Enhancement and Charge Transport Mechanism in Glyme–Lithium Salt Equimolar Complexes. *J. Am. Chem. Soc.* **2011**, *133*, 13121–13129.
- (7) Suo, L.; Borodin, O.; Gao, T.; Olguin, M.; Ho, J.; Fan, X.; Luo, C.; Wang, C.; Xu, K. "Water-in-Salt" Electrolyte Enables High-Voltage Aqueous Lithium-Ion Chemistries. *Science* **2015**, *350*, 938–943.
- (8) Yamada, Y.; Wang, J.; Ko, S.; Watanabe, E.; Yamada, A. Advances and Issues in Developing Salt-Concentrated Battery Electrolytes. *Nat. Energy* **2019**, *4*, 269–280.
- (9) Moon, H.; Mandai, T.; Tatara, R.; Ueno, K.; Yamazaki, A.; Yoshida, K.; Seki, S.; Dokko, K.; Watanabe, M. Solvent Activity in Electrolyte Solutions Controls Electrochemical Reactions in Li-Ion and Li-Sulfur Batteries. *J. Phys. Chem. C* 2015, *119*, 3957–3970.
- (10) Moon, H.; Tatara, R.; Mandai, T.; Ueno, K.; Yoshida, K.; Tachikawa, N.; Yasuda, T.; Dokko, K.; Watanabe, M. Mechanism of Li Ion Desolvation at the Interface of Graphite Electrode and Glyme—Li Salt Solvate Ionic Liquids. *J. Phys. Chem. C* **2014**, *118*, 20246—20256.
- (11) Ren, X.; Chen, S.; Lee, H.; Mei, D.; Engelhard, M. H.; Burton, S. D.; Zhao, W.; Zheng, J.; Li, Q.; Ding, M. S.; Schroeder, M.; Alvarado, J.; Xu, K.; Meng, Y. S.; Liu, J.; Zhang, J.-G.; Xu, W. Localized High-Concentration Sulfone Electrolytes for High-Efficiency Lithium-Metal Batteries. *Chem* **2018**, *4*, 1877–1892.
- (12) Zhang, X.; Jia, H.; Xu, Y.; Zou, L.; Engelhard, M. H.; Matthews, B. E.; Wang, C.; Zhang, J.-G.; Xu, W. Unravelling High-Temperature Stability of Lithium-Ion Battery with Lithium-Rich Oxide Cathode in Localized High-Concentration Electrolyte. *J. Power Sources Adv.* **2020**, *5*, No. 100024.
- (13) Martins, M. L.; Sacci, R. L.; Sanders, N. C.; Tyler, J. L.; Matsumoto, R.; Popov, I.; Guo, W.; Dai, S.; Cummings, P. T.; Sokolov, A. P.; Mamontov, E. Addition of Chloroform in a Solvent-in-Salt Electrolyte: Outcomes in the Microscopic Dynamics in Bulk and Confinement. J. Phys. Chem. C 2020, 124, 22366–22375.
- (14) Dokko, K.; Tachikawa, N.; Yamauchi, K.; Tsuchiya, M.; Yamazaki, A.; Takashima, E.; Park, J.-W.; Ueno, K.; Seki, S.; Serizawa, N.; Watanabe, M. Solvate Ionic Liquid Electrolyte for Li-S Batteries. *J. Electrochem. Soc.* **2013**, *160*, A1304—A1310.
- (15) Doi, T.; Shimizu, Y.; Hashinokuchi, M.; Inaba, M. Dilution of Highly Concentrated LiBF ₄ /Propylene Carbonate Electrolyte Solution with Fluoroalkyl Ethers for 5-V LiNi _{0.5} Mn _{1.5} O ₄ Positive Electrodes. *J. Electrochem. Soc.* **2017**, *164*, A6412–A6416.
- (16) Zheng, J.; Chen, S.; Zhao, W.; Song, J.; Engelhard, M. H.; Zhang, J.-G. Extremely Stable Sodium Metal Batteries Enabled by Localized High-Concentration Electrolytes. *ACS Energy Lett.* **2018**, *3*, 315–321.
- (17) Chen, S.; Zheng, J.; Mei, D.; Han, K. S.; Engelhard, M. H.; Zhao, W.; Xu, W.; Liu, J.; Zhang, J. High-Voltage Lithium-Metal Batteries Enabled by Localized High-Concentration Electrolytes. *Adv. Mater.* **2018**, *30*, No. 1706102.
- (18) Ueno, K.; Murai, J.; Ikeda, K.; Tsuzuki, S.; Tsuchiya, M.; Tatara, R.; Mandai, T.; Umebayashi, Y.; Dokko, K.; Watanabe, M. Li ⁺ Solvation and Ionic Transport in Lithium Solvate Ionic Liquids Diluted by Molecular Solvents. *J. Phys. Chem. C* **2016**, *120*, 15792–15802.
- (19) Martins, M. L.; Sacci, R. L.; Lin, X.; Matsumoto, R.; Popov, I.; Cui, J.; Kobayashi, T.; Tyagi, M.; Guo, W.; Dai, S.; Pruski, M.; Cummings, P. T.; Sokolov, A. P.; Mamontov, E. Beyond Simple Dilution: Superior Conductivities from Cosolvation of Acetonitrile/LiTFSI Concentrated Solution with Acetone. *J. Phys. Chem. C* 2022, 126, 2788–2796.

- (20) Haynes, W. M., Ed. CRC Handbook of Chemistry and Physics, 95th ed.; CRC Press: Boca Raton, 2014.
- (21) Aminabhavi, T. M.; Aralaguppi, M. I.; Harogoppad, S. B.; Balundgi, R. H. Polarizability and Molecular Radius of Bromoform and Hydrocarbon Liquids. *Fluid Phase Equilib.* **1992**, *72*, 211–226.
- (22) Rivelino, R.; Cabral, B. J. C.; Coutinho, K.; Canuto, S. Electronic Polarization in Liquid Acetonitrile: A Sequential Monte Carlo/Quantum Mechanics Investigation. *Chem. Phys. Lett.* **2005**, 407, 13–17.
- (23) Ritzoulis, G.; Papadopoulos, N.; Jannakoudakis, D. Densities, Viscosities, and Dielectric Constants of Acetonitrile + Toluene at 15, 25, and 35.Degree.C. J. Chem. Eng. Data 1986, 31, 146–148.
- (24) Mopsik, F. I. Dielectric Properties of Slightly Polar Organic Liquids as a Function of Pressure, Volume, and Temperature. *J. Chem. Phys.* **1969**, *50*, 2559–2569.
- (25) Liu, Z.; Timmermann, J.; Reuter, K.; Scheurer, C. Benchmarks and Dielectric Constants for Reparametrized OPLS and Polarizable Force Field Models of Chlorinated Hydrocarbons. *J. Phys. Chem. B* **2018**, *122*, 770–779.
- (26) Dang, L. X. Intermolecular Interactions of Liquid Dichloromethane and Equilibrium Properties of Liquid—Vapor and Liquid—Liquid Interfaces: A Molecular Dynamics Study. *J. Chem. Phys.* **1999**, *110*, 10113—10122.
- (27) Barreto, R.; Canuto, S.; Coutinho, K.; Georg, H. C.Molecular Polarization in Liquid Environment. *Trends and Perspectives in Modern Computational Science*; Taylor & Francis, 2006; Vol. 6, p. 80.
- (28) Jorge, M.; Gomes, J. R. B.; Barrera, M. C. The Dipole Moment of Alcohols in the Liquid Phase and in Solution. *J. Mol. Liq.* **2022**, 356, No. 119033.
- (29) Vidulich, G. A.; Kay, R. L. The Dielectric Constant of Water between 0° and 40°. *J. Phys. Chem. A* **1962**, *66*, 383.
- (30) Badyal, Y. S.; Saboungi, M.-L.; Price, D. L.; Shastri, S. D.; Haeffner, D. R.; Soper, A. K. Electron Distribution in Water. *J. Chem. Phys.* **2000**, *112*, 9206–9208.
- (31) Popov, I.; Sacci, R. L.; Sanders, N. C.; Matsumoto, R. A.; Thompson, M. W.; Osti, N. C.; Kobayashi, T.; Tyagi, M.; Mamontov, E.; Pruski, M.; Cummings, P. T.; Sokolov, A. P. Critical Role of Anion—Solvent Interactions for Dynamics of Solvent-in-Salt Solutions. J. Phys. Chem. C 2020, 124, 8457—8466.
- (32) Tang, Z.-K.; Tse, J. S.; Liu, L.-M. Unusual Li-Ion Transfer Mechanism in Liquid Electrolytes: A First-Principles Study. *J. Phys. Chem. Lett.* **2016**, *7*, 4795–4801.
- (33) Tan, P.; Yue, J.; Yu, Y.; Liu, B.; Liu, T.; Zheng, L.; He, L.; Zhang, X.; Suo, L.; Hong, L. Solid-Like Nano-Anion Cluster Constructs a Free Lithium-Ion-Conducting Superfluid Framework in a Water-in-Salt Electrolyte. *J. Phys. Chem. C* **2021**, *125*, 11838—11847.
- (34) Mukherji, S.; Avula, N. V. S.; Kumar, R.; Balasubramanian, S. Hopping in High Concentration Electrolytes Long Time Bulk and Single-Particle Signatures, Free Energy Barriers, and Structural Insights. *J. Phys. Chem. Lett.* **2020**, *11*, 9613–9620.
- (35) Dokko, K.; Watanabe, D.; Ugata, Y.; Thomas, M. L.; Tsuzuki, S.; Shinoda, W.; Hashimoto, K.; Ueno, K.; Umebayashi, Y.; Watanabe, M. Direct Evidence for Li Ion Hopping Conduction in Highly Concentrated Sulfolane-Based Liquid Electrolytes. *J. Phys. Chem. B* 2018, 122, 10736–10745.
- (36) Mamontov, E.; Herwig, K. W. A Time-of-Flight Backscattering Spectrometer at the Spallation Neutron Source, BASIS. *Rev. Sci. Instrum.* **2011**, *82*, No. 085109.
- (37) Martins, M. L.; Gates, W. P.; Michot, L.; Ferrage, E.; Marry, V.; Bordallo, H. N. Neutron Scattering, a Powerful Tool to Study Clay Minerals. *Appl. Clay Sci.* **2014**, *96*, 22–35.
- (38) Arnold, O.; Bilheux, J. C.; Borreguero, J. M.; Buts, A.; Campbell, S. I.; Chapon, L.; Doucet, M.; Draper, N.; Ferraz Leal, R.; Gigg, M. A.; Lynch, V. E.; Markvardsen, A.; Mikkelson, D. J.; Mikkelson, R. L.; Miller, R.; Palmen, K.; Parker, P.; Passos, G.; Perring, T. G.; Peterson, P. F.; Ren, S.; Reuter, M. A.; Savici, A. T.; Taylor, J. W.; Taylor, R. J.; Tolchenov, R.; Zhou, W.; Zikovsky, J. Mantid—Data Analysis and Visualization Package for Neutron

- Scattering and μ SR Experiments. Nucl. Instrum. Methods Phys. Res., Sect. A 2014, 764, 156–166.
- (39) Mamontov, E.; Smith, R. W.; Billings, J. J.; Ramirez-Cuesta, A. J. Simple Analytical Model for Fitting QENS Data from Liquids. *Phys. B* **2019**, *566*, 50–54.
- (40) Ramirez-Cuesta, A. J. T.; Cheng, Y. Q. The ICEMAN, a Heterogeneous Platform for Analysis of Neutron Scattering Data. *Neutron News* **2021**, *32*, 15–16.
- (41) Azuah, R. T.; Kneller, L. R.; Qiu, Y.; Tregenna-Piggott, P. L. W.; Brown, C. M.; Copley, J. R. D.; Dimeo, R. M. DAVE: A Comprehensive Software Suite for the Reduction, Visualization, and Analysis of Low Energy Neutron Spectroscopic Data. *J. Res. Natl. Inst. Stand. Technol.* **2009**, *114*, 341.
- (42) mBuild GitHub Landing Page; GitHub, 2020. https://github.com/mosdef-hub/mbuild (accessed March 15, 2020).
- (43) Klein, C.; Sallai, J.; Jones, T. J.; Iacovella, C. R.; McCabe, C.; Cummings, P. T.A Hierarchical, Component Based Approach to Screening Properties of Soft Matter. In *Foundations of Molecular Modeling and Simulation*; Snurr, R. Q.; Adjiman, C. S.; Kofke, D. A., Eds.; Springer Singapore: Singapore, 2016; pp 79–92.
- (44) Martínez, L.; Andrade, R.; Birgin, E. G.; Martínez, J. M. PACKMOL: A Package for Building Initial Configurations for Molecular Dynamics Simulations. *J. Comput. Chem.* **2009**, *30*, 2157–2164.
- (45) Klein, C.; Summers, A. Z.; Thompson, M. W.; Gilmer, J. B.; McCabe, C.; Cummings, P. T.; Sallai, J.; Iacovella, C. R. Formalizing Atom-Typing and the Dissemination of Force Fields with Foyer. *Comput. Mater. Sci.* **2019**, *167*, 215–227.
- (46) Wang, J.; Wolf, R. M.; Caldwell, J. W.; Kollman, P. A.; Case, D. A. Development and Testing of a General Amber Force Field. *J. Comput. Chem.* **2004**, *25*, 1157–1174.
- (47) Summers, A. Z.; Gilmer, J. B.; Iacovella, C. R.; Cummings, P. T.; MCabe, C. MoSDeF, a Python Framework Enabling Large-Scale Computational Screening of Soft Matter: Application to Chemistry-Property Relationships in Lubricating Monolayer Films. *J. Chem. Theory Comput.* **2020**, *16*, 1779–1793.
- (48) MoSDeF GitHub Landing Page; GitHub, 2020. https://github.com/mosdefhub (accessed March 15, 2020).
- (49) Adorf, C. S.; Dodd, P. M.; Ramasubramani, V.; Glotzer, S. C. Simple Data and Workflow Management with the Signac Framework. *Comput. Mater. Sci.* **2018**, *146*, 220–229.
- (50) Ramasubramani, V.; Adorf, C.; Dodd, P.; Dice, B.; Glotzer, S. In Signac: A Python Framework for Data and Workflow Management, Proceedings of the 17th Python in Science Conference; Akici, F.; Lippa, D.; Niederhut, D.; Pacer, M., Eds.; 2018; pp 152–159.
- (51) Adorf, C. S.; Ramasubramani, V.; Dice, B. D.; Henry, M. M.; Dodd, P. M.; Glotzer, S. C. Glotzerlab/Signac; Zenodo, 2019. DOI: 10.5281/ZENODO.2581327.
- (52) Vanquelef, E.; Simon, S.; Marquant, G.; Garcia, E.; Klimerak, G.; Delepine, J. C.; Cieplak, P.; Dupradeau, F.-Y. Server: A Web Service for Deriving RESP and ESP Charges and Building Force Field Libraries for New Molecules and Molecular Fragments. *Nucleic Acids Res.* **2011**, *39*, W511–W517.
- (53) Canongia Lopes, J. N.; Pádua, A. A. H. CL&P: A Generic and Systematic Force Field for Ionic Liquids Modeling. *Theor. Chem. Acc.* **2012**, *131*, No. 1129.
- (54) Canongia Lopes, J. N.; Deschamps, J.; Pádua, A. A. H. Modeling Ionic Liquids Using a Systematic All-Atom Force Field. *J. Phys. Chem. B* **2004**, *108*, 2038–2047.
- (55) Thompson, M. W.; Matsumoto, R.; Sacci, R. L.; Sanders, N. C.; Cummings, P. T. Scalable Screening of Soft Matter: A Case Study of Mixtures of Ionic Liquids and Organic Solvents. *J. Phys. Chem. B* **2019**, *123*, 1340–1347.
- (56) Abraham, M. J.; Murtola, T.; Schulz, R.; Páll, S.; Smith, J. C.; Hess, B.; Lindahl, E. GROMACS: High Performance Molecular Simulations through Multi-Level Parallelism from Laptops to Supercomputers. *SoftwareX* **2015**, *1*–2, 19–25.
- (57) McGibbon, R. T.; Beauchamp, K. A.; Harrigan, M. P.; Klein, C.; Swails, J. M.; Hernández, C. X.; Schwantes, C. R.; Wang, L.-P.;

- Lane, T. J.; Pande, V. S. MDTraj: A Modern Open Library for the Analysis of Molecular Dynamics Trajectories. *Biophys. J.* **2015**, *109*, 1528–1532.
- (58) Yang, Y.; Takahashi, M.; Kawazoe, Y. Atomic Ordering Recognized by Convergence Characteristics of the Radial Distribution Function. *Solid State Commun.* **2008**, *146*, 468–471.
- (59) Gainaru, C.; Stacy, E. W.; Bocharova, V.; Gobet, M.; Holt, A. P.; Saito, T.; Greenbaum, S.; Sokolov, A. P. Mechanism of Conductivity Relaxation in Liquid and Polymeric Electrolytes: Direct Link between Conductivity and Diffusivity. *J. Phys. Chem. B* **2016**, 120, 11074–11083.
- (60) Wang, Y.; Chen, W.; Zhao, Q.; Jin, G.; Xue, Z.; Wang, Y.; Mu, T. Ionicity of Deep Eutectic Solvents by Walden Plot and Pulsed Field Gradient Nuclear Magnetic Resonance (PFG-NMR. *Phys. Chem. Chem. Phys.* **2020**, 22, 25760–25768.
- (61) Wang, Y.; Fan, F.; Agapov, A. L.; Yu, X.; Hong, K.; Mays, J.; Sokolov, A. P. Design of Superionic Polymers—New Insights from Walden Plot Analysis. *Solid State Ionics* **2014**, *262*, 782–784.
- (62) Lundin, F.; Aguilera, L.; Hansen, H. W.; Lages, S.; Labrador, A.; Niss, K.; Frick, B.; Matic, A. Structure and Dynamics of Highly Concentrated LiTFSI/Acetonitrile Electrolytes. *Phys. Chem. Chem. Phys.* **2021**, 23, 13819–13826.
- (63) Qian, K.; Seifert, S.; Winans, R. E.; Li, T. Understanding Solvation Behavior of the Saturated Electrolytes with Small/Wide-Angle X-Ray Scattering and Raman Spectroscopy. *Energy Fuels* **2021**, 35, 19849–19855.
- (64) Villers, D.; Dosière, M. Subsidiary WAXS Maxima and Morphology of Aliphatic Polyester Crystals Obtained by Crystallization from Solution. *Polymer* 1998, 39, 3129–3134.
- (65) Chaban, V. Competitive Solvation of (Bis)-(Trifluoromethanesulfonyl)Imide Anion by Acetonitrile and Water. Chem. Phys. Lett. 2014, 613, 90–94.
- (66) Dou, Q.; Lei, S.; Wang, D.-W.; Zhang, Q.; Xiao, D.; Guo, H.; Wang, A.; Yang, H.; Li, Y.; Shi, S.; Yan, X. Safe and High-Rate Supercapacitors Based on an "Acetonitrile/Water in Salt" Hybrid Electrolyte. *Energy Environ. Sci.* **2018**, *11*, 3212–3219.
- (67) Kameda, Y.; Saito, S.; Saji, A.; Amo, Y.; Usuki, T.; Watanabe, H.; Arai, N.; Umebayashi, Y.; Fujii, K.; Ueno, K.; Ikeda, K.; Otomo, T. Solvation Structure of Li ⁺ in Concentrated Acetonitrile and *N,N*-Dimethylformamide Solutions Studied by Neutron Diffraction with ⁶ Li/ ⁷ Li Isotopic Substitution Methods. *J. Phys. Chem. B* **2020**, *124*, 10456–10464.
- (68) Do, C.; Sun, X.-G.; Jafta, C. J.; Dai, S.; Ohl, M.; Mamontov, E. Methyl Quantum Tunneling in Ionic Liquid [DMIm][TFSI] Facilitated by Bis(Trifluoromethane)Sulfonimide Lithium Salt. *Sci. Rep.* **2018**, *8*, No. 10354.
- (69) Mamontov, E.; Osti, N. C.; Ryder, M. R. Order-Disorder in Room-Temperature Ionic Liquids Probed via Methyl Quantum Tunneling. *Struct. Dyn.* **2021**, *8*, No. 024303.
- (70) Matsumoto, R.; Thompson, M. W.; Cummings, P. T. Ion Pairing Controls Physical Properties of Ionic Liquid-Solvent Mixtures. *J. Phys. Chem. B* **2019**, *123*, 9944–9955.
- (71) Kovacs, H.; Kowalewski, J.; Laaksonen, A. Molecular Dynamics Simulation of Liquid Mixtures of Acetonitrile and Chloroform. *J. Phys. Chem. B* **1990**, *94*, 7378–7385.
- (72) O'Reilly, D. E.; Peterson, E. M. Self-Diffusion Coefficients and Rotational Correlation Times in Polar Liquids. III. Toluene. *J. Chem. Phys.* **1972**, *56*, 2262–2266.
- (73) Osti, N. C.; van Aken, K. L.; Thompson, M. W.; Tiet, F.; Jiang, D.; Cummings, P. T.; Gogotsi, Y.; Mamontov, E. Solvent Polarity Governs Ion Interactions and Transport in a Solvated Room-Temperature Ionic Liquid. *J. Phys. Chem. Lett.* **2017**, *8*, 167–171.

□ Recommended by ACS

Intermolecular Interactions and Electrochemical Studies on Highly Concentrated Acetate-Based Water-in-Salt and Ionic Liquid Electrolytes

Mona Amiri and Daniel Bélanger

MARCH 23, 2023

THE JOURNAL OF PHYSICAL CHEMISTRY B

Dynamic Heterogeneity of Solvent Motion and Ion Transport in Concentrated Electrolytes

Chao Fang, Rui Wang, et al.

FEBRUARY 17, 2023

THE JOURNAL OF PHYSICAL CHEMISTRY B

READ 🗹

Heterogeneity and Nanostructure of Superconcentrated LiTFSI-EmimTFSI Hybrid Aqueous Electrolytes: Beyond the 21 m Limit of Water-in-Salt Electrolyte

Harender S. Dhattarwal and Hemant K. Kashyap

JULY 12, 2022

THE JOURNAL OF PHYSICAL CHEMISTRY B

READ 🗹

Explicit Polarization in Coarse-Grained Simulations of Ionomer Melts

Christopher Balzer and Amalie L. Frischknecht

NOVEMBER 02, 2022

MACROMOLECULES

READ 🗹

Get More Suggestions >